

# Geophysical Research Letters<sup>®</sup>

## RESEARCH LETTER






10.1029/2025GL119289

## Cycled Fluid Injection Limits Maximum Earthquake Size by Controlling the Cadence of Seismic Moment Release



### Key Points:

- Cyclic injection strategies regulate the cadence of seismic moment, and the total seismic moment is independent of the number of cycles
- Injection–extraction cycles actively reduce pore pressure, temporally partition successive slip events, and suppress delayed seismicity
- The maximum seismic moment is governed by fault structure, stress state, and injected volume

Zhi Geng<sup>1,2,3</sup> , Lei Wang<sup>4</sup> , Quansheng Liu<sup>5</sup> , Junpeng Wang<sup>3</sup> , Pengliang Yu<sup>3</sup> , Yuan Zhou<sup>1,2</sup>, Youqi Huang<sup>6</sup>, Yongshui Kang<sup>1,2</sup>, Bin Liu<sup>1,2</sup> , and Derek Elsworth<sup>3,7</sup> 

<sup>1</sup>State Key Laboratory of Geomechanics and Geotechnical Engineering Safety, Institute of Rock and Soil Mechanics, Chinese Academy of Sciences, Wuhan, China, <sup>2</sup>University of Chinese Academy of Sciences, Beijing, China, <sup>3</sup>Department of Energy and Mineral Engineering, EMS Energy Institute and G3 Center, Pennsylvania State University, University Park, PA, USA, <sup>4</sup>GFZ Helmholtz Centre for Geosciences, Potsdam, Germany, <sup>5</sup>School of Civil Engineering, Wuhan University, Wuhan, China, <sup>6</sup>State Key Laboratory for Geomechanics and Deep Underground Engineering, School of Mechanics and Civil Engineering, China University of Mining and Technology, Xuzhou, China, <sup>7</sup>Department of Geosciences, Pennsylvania State University, University Park, PA, USA

### Supporting Information:

Supporting Information may be found in the online version of this article.

### Correspondence to:

B. Liu,  
liubin@whrsm.ac.cn

### Citation:

Geng, Z., Wang, L., Liu, Q., Wang, J., Yu, P., Zhou, Y., et al. (2026). Cycled fluid injection limits maximum earthquake size by controlling the cadence of seismic moment release. *Geophysical Research Letters*, 53, e2025GL119289. <https://doi.org/10.1029/2025GL119289>

Received 5 SEP 2025  
Accepted 27 JAN 2026

### Author Contributions:

**Conceptualization:** Zhi Geng, Derek Elsworth  
**Data curation:** Zhi Geng, Derek Elsworth  
**Formal analysis:** Zhi Geng, Derek Elsworth  
**Funding acquisition:** Bin Liu  
**Investigation:** Zhi Geng, Lei Wang, Junpeng Wang, Pengliang Yu, Youqi Huang, Derek Elsworth  
**Resources:** Zhi Geng, Lei Wang, Quansheng Liu, Yuan Zhou, Yongshui Kang  
**Software:** Lei Wang  
**Supervision:** Lei Wang  
**Validation:** Zhi Geng, Derek Elsworth  
**Visualization:** Lei Wang  
**Writing – original draft:** Zhi Geng

**Abstract** Controlling fluid injection is widely considered a key to limiting the size of injection-induced seismicity, yet whether and how it limits earthquake size remains debated. We perform injection-reativation experiments on critically stressed faults to test how different injection strategies shape slip and seismic moment release. We find that injection strategies regulate the cadence of slip events rather than the total seismic moment. Compared to continuous injection, cycled injection triggers frequent and smaller events, reducing maximum moment magnitude and deformation energy of individual events. Injection–extraction cycles actively reduce pore pressure, temporally partition successive slip events, and effectively suppress delayed seismicity. Regardless of constant or cycled injection rates, maximum seismic moment ( $M_0$ ) scales with cumulative injection volume ( $\Delta V$ ) (i.e.,  $M_0 \propto \Delta V^{3/2}$ ). Our laboratory results suggest that regulating the cadence of moment release promotes effective hazard mitigation.

**Plain Language Summary** Fluid injection–related industrial operations have been found to be linked to induced seismic activity. To date, it remains controversial whether it is possible to reduce the maximum magnitude of induced earthquakes by adjusting injection operations. Here, our laboratory experiments show that, under conditions of equal injected volume and critical stress, different strategies regulate the cadence of slip events rather than the total seismic moment. Continuous injection produces less but larger slip events, while cycled injection triggers more frequent and smaller events. Injection–extraction cycles temporally partition events and suppress delayed earthquakes. We also present a predictive model for the maximum seismic moment across laboratory and field scales, showing that the magnitude of earthquake is controlled by injected volume and fault conditions.

## 1. Introduction

Fluid injection associated with industrial activities such as geothermal energy extraction, shale gas production, CO<sub>2</sub> sequestration, and wastewater disposal has been widely linked to induced seismicity (Atkinson et al., 2020; Ellsworth, 2013; Elsworth et al., 2016; McGarr et al., 2015). Notable injection-triggered events include the  $M_w$  5.8 Pawnee earthquake in Oklahoma (Kolawole et al., 2019) and the  $M_w$  5.4 Pohang earthquake (Kim et al., 2018; Figure 1a), indicating inadequate control during fluid injection operations. Various potential triggering mechanisms have been proposed, including pore pressure diffusion (Kang et al., 2019), pore-elastic stress changes (Ellsworth, 2013; Ji, Wang, et al., 2022), and interactions between faults mediated by seismic or static stress transfer (Bao & Eaton, 2016; Garagash & Germanovich, 2012). While the link between fluid injection and seismicity is now well established, not all injection operations induce earthquakes. Earthquake magnitude and seismic moment release were reported to be constrained by injection strategies (Li et al., 2021). To mitigate seismic risk, injection strategies are commonly optimized by adjusting parameters such as injection rate (Alghannam & Juanes, 2020; Wang, Kwiatek, Rybacki, Bonnelye, et al., 2020), pore pressure rise (Mandal & Lui, 2022), cumulative volume (McGarr & Barbour, 2018), and injection rate periodicity (Evans et al., 2012). Laboratory and field studies have shown that well-designed injection strategies can limit seismic moment release, thereby constraining fault rupture and earthquake nucleation and reducing the risk of large earthquakes (Ji

© 2026. The Author(s).

This is an open access article under the terms of the [Creative Commons Attribution License](https://creativecommons.org/licenses/by/4.0/), which permits use, distribution and reproduction in any medium, provided the original work is properly cited.

Writing – review & editing: Zhi Geng,  
Lei Wang, Derek Elsworth

et al., 2021; Zang et al., 2013; Zhu et al., 2021). Although the relationship between injection parameters and cumulative seismic moment has been extensively studied, whether and how different injection strategies (e.g., changes in injection pressure, pressurization rate, and injection periodicity) affect seismic moment release and the cadence of fault slip, particularly under critically stressed conditions and controlled injection volume, remains unclear.

Recent studies suggest that cyclic injection, such as periodic injection separated by shut-in intervals, can reduce the risk of large earthquakes by promoting a sequence of smaller slip events instead of a single large rupture (Ji et al., 2021; Niemz et al., 2020; Zang et al., 2013, 2019; Zhuang et al., 2019; Zhu et al., 2021). However, geothermal projects in Basel and Pohang have shown that the largest magnitude events occurred during the shut-in period rather than within the injection period, revealing limitations of this strategy (Häring et al., 2008; Yeo et al., 2020). Follow-up studies have found that high pore pressure can continue to diffuse within fault zones during the shut-in period, reactivating critically stressed fault surfaces and potentially triggering delayed seismic events, with such trailing earthquakes exhibiting time lags ranging from several months to years (Guglielmi et al., 2015). This phenomenon has prompted the re-evaluation of the effectiveness of injection strategies, particularly to suppress seismic slip during shut-in periods. This is necessary to achieve effective decoupling of slip processes between successive injection stages, which remains a critical challenge. Although some studies have proposed gradually reducing the pore pressure during the pressure-hold phase to dampen stress perturbations and to mitigate early post-injection fault instability (Alghannam & Juanes, 2020; Boyet et al., 2024; Boyet et al., 2023), the coupled mechanisms linking pressurization rate evolution with shear stress regulation, fault unloading stiffness changes, and seismic moment release remain poorly understood and require systematic experimental validation and theoretical investigation.

Here, we conducted a series of injection-reativation experiments to investigate the effects of different injection strategies on fault mechanical response, evolution of slip stability, and the associated characteristics of seismic moment release (Figure 1). We show that different injection strategies can significantly regulate the slip cadence and rate of seismic moment release while the total seismic moment releases remain similar. We propose a new cyclic injection and extraction strategy that actively reduces pore pressure during shut-in periods, potentially reducing the likelihood of triggered seismicity. We further propose a real-time seismic moment theoretical model that integrates injection parameters and fault mechanical properties. These observations show that injection parameters and fault slip mechanical properties control rates of energy release in a predictable manner.

## 2. Materials and Methods

### 2.1. Rock Samples and Experimental Procedures

Eight samples were cored from high-permeability homogeneous sandstone (porosity  $\approx 16.6\%$ , permeability  $\approx 10^{-12} \text{ m}^2$ ) blocks to minimize the heterogeneity in stress and pore pressure conditions. Each specimen was a cylindrical core (50 mm in diameter and 100 mm in length), with a precut fault plane inclined at  $\varphi = 30^\circ$  to the axial direction. The fault surfaces were uniformly ground with 80-grit sandpaper (average particle size  $\sim 200 \mu\text{m}$ ) to ensure consistent roughness, resulting in room-mean-square (rms) roughness of about  $35 \mu\text{m}$ . All experiments were conducted under a confining pressure of  $\sigma_3 = 35 \text{ MPa}$  and an initial pore pressure of  $4 \text{ MPa}$ . Axial loading was applied until reaching peak shear stress ( $\tau_{ss}$ ), then decreased at a rate of  $0.05 \text{ MPa/min}$  to approximately  $0.9 \tau_{ss}$  before locking the piston, after which fluid pressurization was initiated.

Fluid injection was pressure-controlled, with net pore pressure increasing from  $4$  to  $28 \text{ MPa}$  in all tests. Theoretical total injection volume (approximately  $3.6 \text{ mL}$ ) and injection duration ( $24 \text{ min}$ ) were kept constant across all tests. Eight injection schemes were designed: Scheme 1 employed continuous injection at  $1 \text{ MPa/min}$ ; Schemes 2 to 5 used shut-in cycling injection with 3, 6, 12, and 24 total cycles, respectively, each at an injection rate of  $2 \text{ MPa/min}$  (variable-periodicity, constant-rate). Schemes 6 to 8 used injection–extraction cycling, all with 12 cycles comprising equal-duration injection and extraction phases (constant-periodicity, variable-rate). Injection rates were set at 4, 6, and  $8 \text{ MPa/min}$ , respectively, with corresponding extraction rates of 2, 4, and  $6 \text{ MPa/min}$ . Throughout the experiments, we simultaneously monitored shear mechanical responses, slip behavior, stability, acoustic emission (AE) activity and the associated seismic energy release. This study focuses on how different injection strategies, under fixed injection volume and critical stress conditions, regulate the cadence of fault slip seismic moment release. Although the total injected volume was desired identical across experiments, slight variations in total injected volume arose due to the coupling between instantaneous flow rate and pore

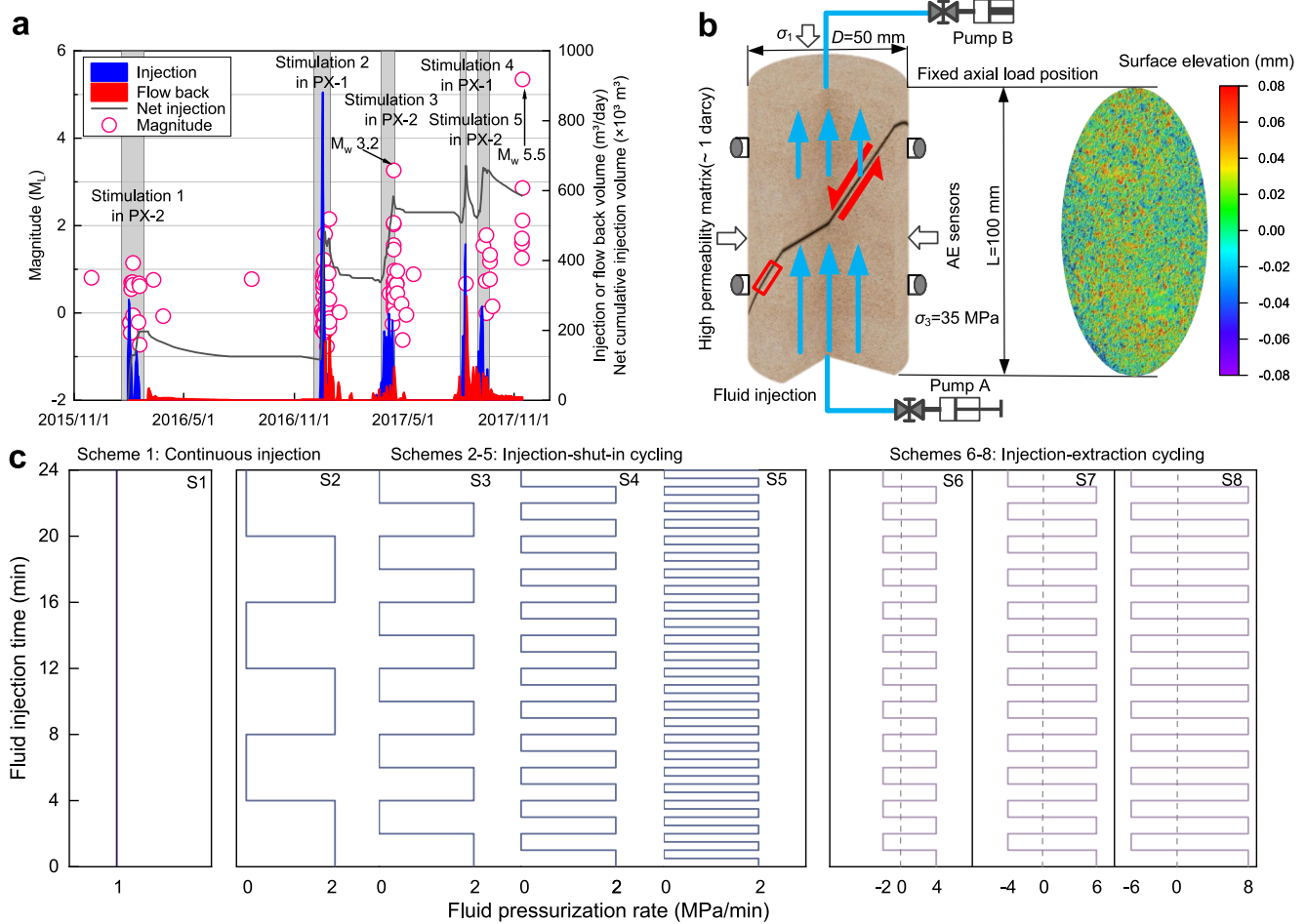


**Figure 1.** Fluid injection strategies and seismic responses. (a) Temporal evolution of injection volumes and seismic magnitudes during multi-stage hydraulic stimulations at Pohang geothermal field (adapted from Yeo et al., 2020). Pink circles denote earthquake magnitudes. Blue, red, and black correspond to injection volume, flow-back volume, and net cumulative injection, respectively. (b) Schematic representation of the laboratory injection-induced fault slip experiment. Fluid is injected through a highly permeable matrix (~1 darcy) into a critically stressed fault under a given confining pressure and axial load. Four acoustic emission (AE) sensors were used to detect microseismic events. The right panel shows the profile of the fault surface, which was uniformly roughened using sandpaper to ensure consistent surface roughness. (c) Experimental schemes illustrating three fluid injection strategies: continuous injection (Scheme 1), injection-shut-in cycling (Schemes 2–5), and injection-extraction cycling (Schemes 6–8).

pressure. This mismatch is <5% of the total injected volume and thus negligible (Figure S7a in Supporting Information S1).

## 2.2. Data Processing and Analysis

The specific calculations for stress, seismic-related energy, and slip displacement are provided in Texts S1–S4 of Supporting Information S1. In these derivations, we assume that the pore fluid pressure is spatially uniform along the fault. The detailed procedures for acoustic emission (AE) data processing are given in Text S5 of Supporting Information S1. The full derivation of the maximum seismic moment model is presented in Text S6 of Supporting Information S1.

## 3. Results

### 3.1. Fault Mechanical Response to Varying Fluid Injection Strategies

Fault reactivation during loading occurs in three stages (Text S7, Figure S4 in Supporting Information S1 and Figure 2). Different injection strategies cause marked differences in fault slip patterns and slip cadence (Figures 2, 3a, and 3b). Injection schemes all involve the same average rate of injection but explore the impact of continuous

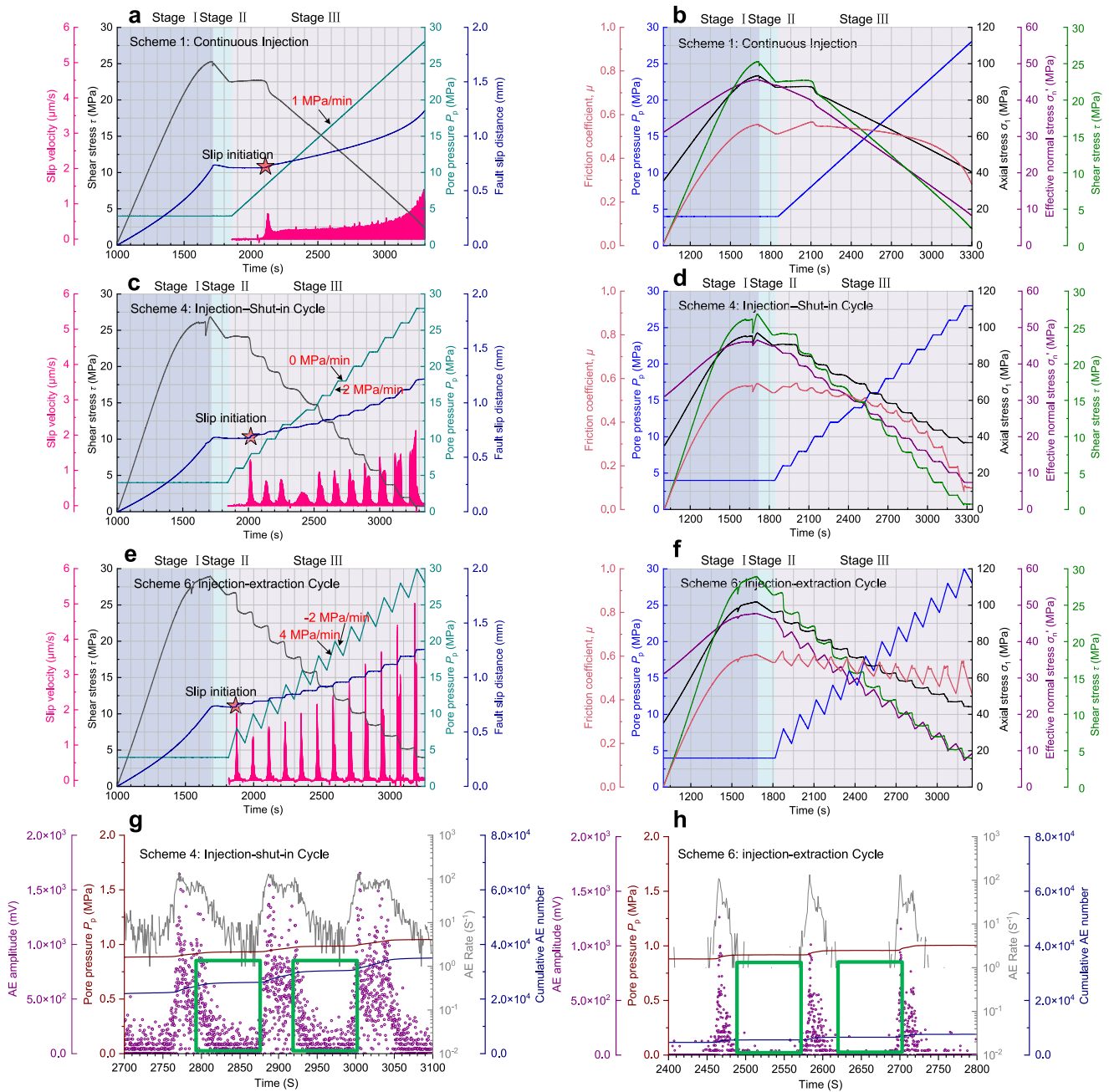


**Figure 2.** Influence of three typical fluid injection strategies on fault slip mechanics, slip mode, frictional behavior, and AE characteristics. (a, c, and e) Temporal evolution of slip velocity, shear stress, pore pressure, and fluid slip distance under three injection schemes: (a) continuous injection (Scheme 1), (c) injection-shut-in (Scheme 4), and (e) injection-extraction cycles (Scheme 6). (b, d, and f) Corresponding changes in fault friction coefficient, shear stress, effective normal stress, axial stress, and pore pressure. (g-h) High-resolution views of acoustic emission (AE) responses for Scheme 4 (g) and Scheme 6 (h), illustrating the temporal evolution of AE magnitude, AE rate, cumulative AE number, and pore pressure.

and cycled injections, including different periodicities and amplitudes (Figure S2 in Supporting Information S1). Continuous injection (Scheme 1) triggers a single large and continuous slip event, releasing most of the strain energy at once (Figure 2). In contrast, injection-shut-in cycling at constant maximum rate but at periodicities decreasing from 8 min (Scheme 2) to 1 min (Scheme 5) partitions slip into multiple, intermittent and small slip events, producing a stepwise decrease in shear stress. As the number of cycles increases from 3 to 24, peak slip decreases slightly from about 2.86  $\mu\text{m/s}$  to 2.13  $\mu\text{m/s}$  (Figure S7d in Supporting Information S1), while slip behavior transitions toward more frequent and smaller slip events. This trend suggests that high numbers of

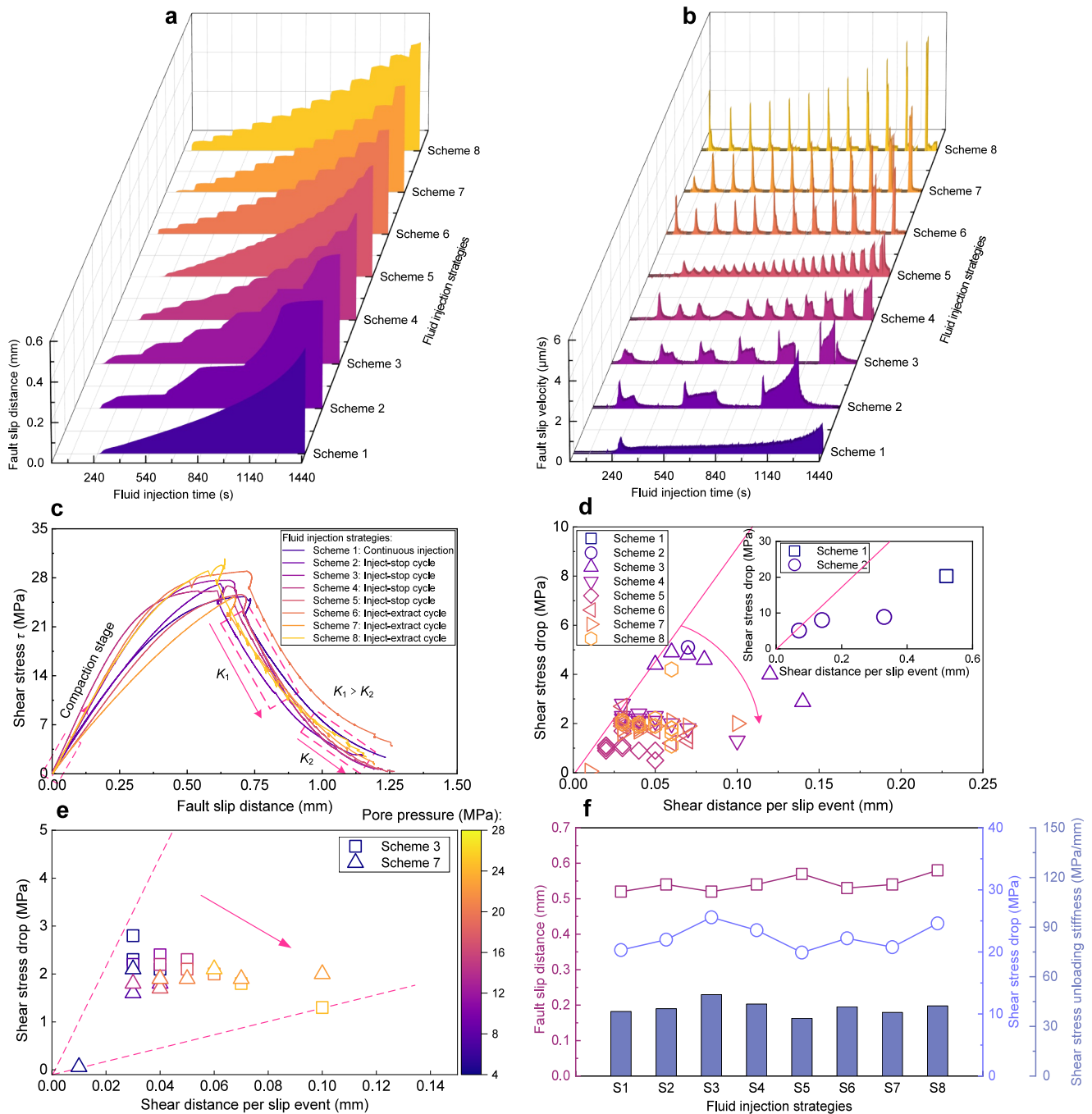


**Figure 3.** Effects of fluid injection strategies on fault slip behavior and rupture characteristics. Panels (a, b) show the temporal evolution of fault slip distance and slip velocity under different injection strategies since the onset of fluid injection. The results suggest that the fluid injection strategy reshapes the cadence and mode of fault slip. Notably, the total fault displacement remains unaffected by the injection strategy. Panel (c) shows the evolution of shear stress with slip distance. The results indicate that the trend of unloading stiffness remains generally consistent across different fluid injection strategies (see texts for details). Panel (d) illustrates the relationship between shear stress drop and slip distance for individual events. Panel (e) compares rupture responses under increasing pore pressure for shut-in cycling (Scheme 3) and injection–extraction cycling (Scheme 7), showing that unloading stiffness decreases progressively with pore pressure, reaching a maximum during the first rupture event. Panel (f) summarizes the total slip and total stress drop, indicating that injection strategy does not significantly alter the average unloading stiffness of the faults (indicated by blue bar graph).

injection cycles suppress large ruptures and promote stable fault slip. Concurrently, as the number of cycles increases, the originally concentrated fault slip is partitioned into more frequent but smaller events, indicating that the injection strategy effectively regulates the cadence of fault slip for a nearly unchanged total seismic moment

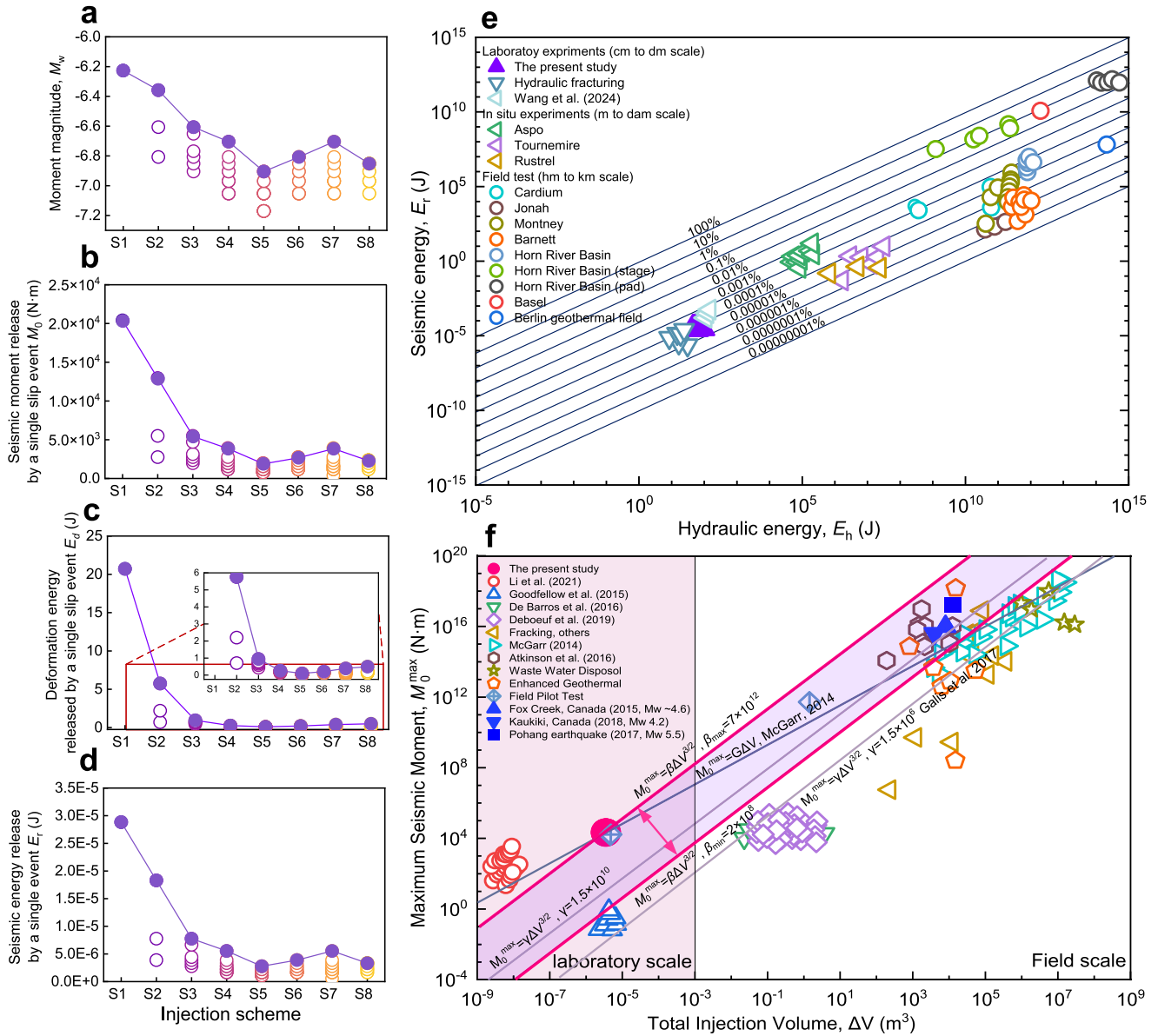


**Figure 4.** Seismic moment, associated energy release, and moment magnitude evolution, and comparison of maximum seismic moment under different injection strategies with field-scale induced earthquakes. (a–d) Quantitative comparisons of seismic responses across eight injection schemes, including moment magnitude of individual slip events (a), seismic moment (b), deformation energy (c), and seismic energy release (d) with the maximum value (purple line) under each strategy indicated. (e) Relationship between seismic energy ( $E_s$ ) and hydraulic energy ( $E_h$ ), combining results from this study and previous field data. Dashed lines indicate constant  $E_s/E_h$  ratios, reflecting injection efficiency. (f) Cross-scale relationship between maximum seismic moment and total injection volume. Red symbols represent laboratory results from this study; other colored symbols correspond to previous field-scale studies. Blue symbols mark three major uncontrolled induced earthquake events. Background shaded region and model curves reflect theoretical constraints and the  $\beta$  range derived in this study.

release. Notably, when the number of cycles exceeds 12 (Schemes 4 and 5), slip continues over successive injection cycles, slip persists during the pore-pressure hold phases without fully stopping, thereby exhibiting quasi-continuous slip between successive cycles.

In contrast, injection-extraction cycling (Schemes 6–8) effectively disrupts slip continuity. Although average injection rates are maintained constant and periodicity is held constant at 2 min, the fluid pressurization rates successively increase x2, then x3 and x4, requiring fluid extraction in the former shut-in phase (Figure 1c and Figure S2 in Supporting Information S1). Compared to the injection-shut-in strategy, fluid extraction periods effectively suppress both fault slip and AE activity (see the green rectangles in Figures 2g and 2h). Although the

operational requirements for field application of this strategy are relatively complex, this approach demonstrates enhanced controllability of slip and stronger suppression of rupture propagation.

The total slip displacement remains nearly constant across all injection scenarios (Schemes 1–8) at  $\sim 0.55$  mm (Figures 3a and 3f), yet the peak slip velocity and cadence of intermittent slip vary significantly, indicating that the fluid injection strategy alters the mode of fault slip rather than the total slip distance. Across all injection schemes, from continuous (Schemes 1) through variable-period, constant-peak-rate (Schemes 2–5) and finally for constant-period, variable-peak-rate (Schemes 6–8), peak slip velocity is linearly correlated with the fluid pressurization rate (Figure S7c in Supporting Information S1). This suggests that fault slip behavior is governed by the fluid pressurization rate rather than injection pressure, consistent with previous studies (Wang, Kwiatek, Rybacki, Bonnelye, et al., 2020). Most events exhibit a sudden increase in slip rate at the beginning, followed by a rapid decay by  $\sim 50\%$  (Figures S4 and S9 in Supporting Information S1). These results suggest that slip initiation is potentially unstable; however, elevated pore pressure alone is insufficient to sustain dynamic rupture propagation. Instead, slip velocity decays rapidly due to limited stress transfer, consistent with both in situ observations and laboratory experiments (Cappa et al., 2019; Guglielmi et al., 2015). Furthermore, under low fluid pressurization rates ( $\leq 2$  MPa/min), the pore pressure triggering fault reactivation remains at  $\sim 8$  MPa (Figure S7b in Supporting Information S1), suggesting that the magnitude of fluid pressure controls fault slip initiation. This indicates that the reactivation threshold is independent of fluid pressurization rate and injection strategy, as observed previously (Wang, Kwiatek, Rybacki, Bonnelye, et al., 2020). In contrast, under increased fluid pressurization rates (Schemes 7–8, with pressurization rate ranging from 6 to 8 MPa/min), we do not observe the delayed triggering phenomenon, in contrast to schemes of low fluid pressurization rate (Figure S7b in Supporting Information S1). In addition, we also conducted acoustic emission (AE) analyses and microscopic observations, with details provided in the Supporting Information (Text S9 in Supporting Information S1).

### 3.2. Evolution of the Friction Coefficient and Stability

We evaluate the friction coefficient  $\mu = \tau/\sigma_h$  from the ratio of shear stress to effective normal stress, assuming uniform pressurization for the different fluid injection strategies. This reveals distinct fault stability responses under different fluid injection strategies (Figure S5 in Supporting Information S1). Given the high permeability of the rock matrix, we assume a spatially uniform distribution of pore pressure when estimating effective stress and friction. In all experiments, the observed friction coefficient increased steadily during axial loading, reaching a peak at  $\sim 0.51$ – $0.62$  (Figures S5 and S7a in Supporting Information S1), consistent with Byerlee's law (Byerlee, 1978), and subsequently increased as pore pressure was increased. Once reactivation occurs, it exhibits an overall decreasing trend. Under continuous injection (Scheme 1), the friction coefficient  $\mu$  progressively declined after reactivation, eventually stabilizing at a residual value of  $\sim 0.25$ . In contrast, injection–shut–in cycling (Schemes 2–5) exhibited minor increases during each fluid pressurization phase and then followed by slow decay and stabilization during the shut-in period. With an increasing number of pressurization cycles, the magnitude of frictional weakening became more pronounced, with residual friction varying from about 0.31 to  $< 0.10$  (Figures S5b–S5e in Supporting Information S1). This suggests that a high number of injection cycles may induce additional weakening mechanisms that progressively reduce the capacity for frictional recovery (Violay et al., 2015). Injection–extraction cycling at constant periodicity but increasing peak rate (Schemes 6–8) demonstrated a stronger ability to regulate fault stability. The evolution of the friction coefficient exhibited a characteristic sawtooth-like cyclic pattern. That is, during each pore pressure loading and unloading phase, the friction coefficient decreases and then recovers, accompanied by circumferential fault dilation and compaction (Figures S6f–S6h in Supporting Information S1). The friction coefficient oscillated within a bounded range and gradually decayed. Ultimately, the residual friction coefficient remained above 0.2.

Total shear stress drop (22.5–27.5 MPa) and cumulative slip distance ( $\sim 0.51$ – $0.55$  mm) are comparable across all experiments (Figure 3f). Such results suggest that fault unloading stiffnesses (i.e., the slope of shear stress drop versus slip distance) associated with slip events in our tests are independent of the injection strategy. The average system stiffness  $K_{\text{sys}}$  is estimated to be  $\sim 83$  MPa/mm (Text S3 in Supporting Information S1). Under all experimental conditions, the average unloading stiffness of the fault (i.e.,  $K_{\text{fault}} \approx 35$ – $49$  MPa/mm), as well as the maximum real-time unloading stiffness observed during reactivation (i.e.,  $K_{\text{fault}}^{\text{max}} \approx 71$  MPa/mm), remains lower than the system stiffness (Figures 3c and 3d), which means that all faults exhibit stable sliding. During progressive loading and slip, further analysis reveals that the unloading stiffness of each slip event reaches a peak at the onset

of slip activation and then gradually decreases (Figure 3e), suggesting that instability is most likely to occur during the early stages of activation (Text S8 in Supporting Information S1).

## 4. Discussion

### 4.1. Release of Energy and Seismic Moment

Under different fluid injection strategies, the fault exhibits marked differences in seismic moment release, moment magnitude, and associated energy evolution characteristics (see Text S2 for calculations of hydraulic energy and slip event-related energy). Hydraulic energy ( $E_h$ ) yields values  $\leq 10^2$  J at all experimental conditions (Figure S6 in Supporting Information S1). The total cumulative seismic moment ( $M_0$ ) across all experiments is of the order of  $2.1 \times 10^4$  N·m, with corresponding total cumulative seismic energy ( $E_s$ ) of approximately  $3.0 \times 10^{-5}$  J (Figures S3g and S3h in Supporting Information S1). These results indicate that under critical stress conditions and constant injection volume, both the total seismic energy and seismic moment are primarily governed by the injected volume and are largely independent of injection periodicity or peak injection rate. Further analysis reveals that during the initial fluid pressurization stage, the seismic moment ( $M_0$ ) exhibits a cubic dependence on the net injected volume ( $\Delta V$ ), as  $M_0 \propto (\Delta V)^3$ , transitioning to a linear trend upon full fault reactivation (Figure S8b in Supporting Information S1). The cumulative seismic moment release remains below McGarr's theoretical limit (McGarr et al., 2015; Figures S8a and S8b in Supporting Information S1), suggesting that slip remained stable and controlled, in agreement with earlier laboratory observations (De Barros et al., 2019; Wang, Kwiatek, Rybacki, Bohnhoff, & Dresen, 2020).

Despite comparable total seismic moment release across all injection modalities, different injection strategies exerted a significant influence on the moment release rate, energy release cadence, and moment magnitude of individual events. The peak seismic moment release rates ranged from  $\sim 69$  to  $\sim 234$  N·m/s and increased markedly with higher fluid pressurization rates (Figure S3 in Supporting Information S1). The moment magnitudes ( $M_w$ ) varied from  $-6.18$  under continuous injection (Scheme 1) to  $-6.93$  under 24-cycle injection (Scheme 5; Figure 4a), consistent with previous laboratory experiments (McGarr, 1999; McLaskey & Kilgore, 2013). With increasing injection cycles, the seismic moment ( $M_0$ ), seismic energy ( $E_s$ ), and deformation energy ( $E_d$ ) released per slip event progressively decreased (Figures 4b, 4d, and 4c). Under continuous injection (Scheme 1), the maximum releases for a single slip event were  $2.92 \times 10^{-5}$  J for seismic energy, 21.3 J for deformation energy, and 21520 N·m for seismic moment. In contrast, for 24-cycles of injection (Scheme 5), the corresponding values dropped to  $3.5 \times 10^{-6}$  J, 0.31 J, and 1840.4 N·m, representing reductions by factors of 8.4, 68.7, and 11.7, respectively. Under injection–extraction cycling, the observed values are comparable to those obtained with only injection (Schemes 4 and 5). While the injection strategy markedly influenced the pattern of energy release, the total seismic energy and moment remained nearly unchanged. This suggests that under controlled stress and volume conditions, fluid injection strategies primarily regulate the cadence of energy release rather than the total seismic moment.

We use “injection efficiency” (Maxwell, 2013), defined as the ratio of radiated seismic energy to hydraulic energy ( $E_r/E_h$ ) to further assess the efficiency of energy release and system stability. Across all experiments, injection efficiency ranged from  $10^{-7}$  to  $10^{-6}$  (Figure 4e and Figure S8c in Supporting Information S1), consistent with values reported in previous laboratory fluid injection and hydraulic fracturing experiments, in situ injection studies, and documented induced seismicity events (Bentz et al., 2020; De Barros et al., 2019; Goodfellow et al., 2015; Wang et al., 2024). These values are significantly below the commonly assumed rupture-risk threshold of  $10^{-3}$  (De Barros et al., 2019; Goodfellow et al., 2015), indicating pressure-dependent rupture process associated with fluid injection.

### 4.2. Injection Strategies Limit the Maximum Size of Induced Seismicity

Our results are highly consistent with previous laboratory and field observations (Ji et al., 2021; Zang et al., 2013; Zhuang et al., 2019; Zhu et al., 2021). Background stress and initial fault conditions determine the upper limits of releasable energy and total seismic moment, while the injection strategy alters the rhythm of moment release rather than the total amount (Li et al., 2021). Compared to continuous injection, cyclic injection (including both shut-in and injection–extraction cycling) can effectively disperse strain release and reduce the magnitude and associated seismic energy of individual slip events. Furthermore, monitoring reveals sustained microseismic

activity during shut-in periods. This activity is likely driven by pore pressure diffusion and is consistent with field and laboratory observations of delayed rupture mechanisms (Goebel & Brodsky, 2018; Kim et al., 2018; Kolawole et al., 2019). Notably, cyclic injection–extraction is demonstrated to mitigate such delayed seismic activity and prevent the occurrence of trailing earthquakes. Its innovation lies in the active reduction of pore pressure, which forcibly restores fault strength and isolates successive slip events. This regulatory mechanism has been previously validated in early controlled field experiments (Raleigh et al., 1976), where alternating “injection–extraction” operations were shown to reduce seismicity rate and enhance system controllability.

Evidence and theory suggest that the relationship between induced seismic moment ( $M_0$ ) and injection volume ( $\Delta V$ ) may conform to a nonlinear power-law trend rather than a simple linear scaling (Galis et al., 2017; van der Elst et al., 2016). Our experiments similarly reveal that the seismic moment accumulates slowly during the initial phase of fluid injection and then increases rapidly once a critical condition is reached, exhibiting a behavior more consistent with a power-law relationship. This trend aligns with the conceptual model that differentiates between contained and uncontained rupture regimes (Galis et al., 2017), depending on whether the seismic moment release surpasses a critical energy threshold in response to a given hydraulic energy input. The delayed accumulation and abrupt release of seismic moment observed in our experiments reflect this mechanism and help to explain why larger events tend to occur only after the injection volume surpasses a threshold. Furthermore, our results show that once the fault transitions from a locked state to a stable-sliding state, the injected energy is mainly released as shear deformation, yielding an approximately linear relationship between  $M_0$  and  $\Delta V$ . In contrast, during the early nucleation phase, when the fault remains locked or subcritically stressed, energy release is delayed and the contribution of early fluid input to seismic moment is limited. Applying a linear model in this regime could overestimate seismic hazard to some extent.

Equating the moment to the stress drop recovered from the volume surrounding a fault to the volume injected solely within the fault zone (Elsworth et al., 2016; Li et al., 2021; J. Yu et al., 2024; P. Yu et al., 2024; Zhu et al., 2021), we recover:  $M_0 = \beta \Delta V^{3/2}$  with  $\beta = (16\xi/7\pi^{3/2}) \cdot (K_{\text{fault}}/\sqrt{h})$  (see Text S6 and Figure S14 in Supporting Information S1 for details) where  $\beta$  is a scaling coefficient,  $h$  is the fault zone thickness,  $\Delta V$  is the injected fluid volume,  $K_{\text{fault}}$  represents the unloading stiffness of the fault, and  $\xi$  denotes the slip ratio (approximated as uniform shear strain across the fault). By integrating fault geometry, mechanical state, slip behavior, and injected volume, the model predicts a nonlinear seismic moment that couples geometric, mechanical, and hydraulic factors. It defines the conditions constraining the upper bound of seismic moment and significantly extends the classical power-law scaling (Galis et al., 2017; Sáez et al., 2025). The model reveals that the maximum seismic moment is primarily constrained by fault geometric and mechanical properties, together with the total injected volume, rather than by the specific injection path or loading protocol, such as fluid pressurization rate, cycling numbers.

Building on established theoretical frameworks (Galis et al., 2017; Li et al., 2021; McGarr, 2014; Sáez et al., 2025; J. Yu et al., 2024; P. Yu et al., 2024), systematic laboratory and field observations, and physically reasonable assumptions, we define the magnitude of the proportionality coefficient  $\beta$ , and constrain its valid range across scales, from laboratory to field, between  $2.0 \times 10^8$  and  $7.0 \times 10^{12}$ , as indicated by the shaded region in Figure 4. This model not only accurately reproduces the seismic moment evolution observed in laboratory experiments, but also successfully accounts for several large-scale injection-induced earthquakes that exceed the McGarr theoretical (McGarr, 2014; McGarr et al., 2015) upper bound, including the 2017 Mw 5.5 Pohang earthquake (Kim et al., 2018), the Mw  $\sim 4.6$  Fox Creek earthquake in Canada, and the Mw 4.2 Kaukiki event. This cross-scale validation highlights the strong potential of the model for seismic hazard assessment and risk mitigation.

### 4.3. Implications for Seismic Hazard Mitigation

We propose that regulating the cadence and rate of seismic moment release is as important as controlling its total amount. For critically stressed reservoirs or those with a history of induced seismicity, injection–extraction cycling may be prioritized. Considering practical operation and economic efficiency, we do not advocate mechanically implementing frequent injection–production cycles in large-scale projects. Instead, we propose conceptualizing “injection–production cycling” as a controllable “pressurization–depressurization cycle,” whereby stopping injection and allowing pore pressure to diffuse (with limited active depressurization if necessary) are used to actively

manage the effective stress state. By increasing the number of cycles and reducing the fluid pressurization rate, this strategy helps mitigate the risk of earthquake triggering and effectively suppresses the occurrence of trailing events. When combined with real-time seismic moment and multi-parameter monitoring such as microseismic activity and fluid operational parameters, this approach enables prompt optimization of injection parameters, thereby enhancing system stability and operational controllability. Furthermore, a traffic-light-style early warning system based on these real-time indicators can provide a scientifically grounded and quantitatively informed basis for fluid injection decision-making. It is important to emphasize that no engineering strategy based on pore pressure management can be considered an absolutely safe solution. Its applicability and boundary conditions must be systematically constrained by the site-specific geological structure, fault geometry, real-time monitoring, and probabilistic risk assessment. If a fault is already near a critical stress state, even well-regulated operations may initiate high-risk events. Therefore, future design of injection protocols and risk thresholds must be grounded in system-level assessments that integrate site-specific tectonic and fault conditions, avoiding an overreliance on operational parameters alone to ensure robust control over induced seismicity.

## 5. Conclusions

In summary, we conducted laboratory fluid injection reactivation experiments to investigate how different injection strategies influence the cadence of fault slip behavior, seismic moment release, and earthquake magnitude. Under fixed injection volumes and critical stress conditions, we find that injection strategy significantly modulates the spatiotemporal cadence of slip, the rate of seismic moment release, and the peak moment magnitude, without altering the total cumulative seismic moment. Continuous injection tends to produce abrupt energy release and larger-magnitude events, whereas shut-in cycling discretizes energy release and effectively reduces the size of individual slip episodes. Injection–extraction cycling further enhances control over fault slip, with periodic unloading suppressing trailing rupture and reducing the clustering and unpredictability of triggered events. We established a multi-scale model for the upper limit of maximum seismic moment and showed that the maximum seismic moment of an event follows the power scaling relation with the injection volume.

## Conflict of Interest

The authors declare no conflicts of interest relevant to this study.

## Data Availability Statement

The experimental data presented in this study are available in Geng (2025).

## References

- Alghannam, M., & Juanes, R. (2020). Understanding rate effects in injection-induced earthquakes. *Nature Communications*, *11*(1), 3053. <https://doi.org/10.1038/s41467-020-16860-y>
- Atkinson, G. M., Eaton, D. W., & Igonin, N. (2020). Developments in understanding seismicity triggered by hydraulic fracturing. *Nature Reviews Earth and Environment*, *1*(5), 264–277. <https://doi.org/10.1038/s43017-020-0049-7>
- Bao, X., & Eaton, D. W. (2016). Fault activation by hydraulic fracturing in Western Canada. *Science*, *354*(6318), 1406–1409. <https://doi.org/10.1126/science.aag2583>
- Bentz, S., Kwiatek, G., Martínez-Garzón, P., Bohnhoff, M., & Dresen, G. (2020). Seismic moment evolution during hydraulic stimulations. *Geophysical Research Letters*, *47*(5), e2019GL086185. <https://doi.org/10.1029/2019GL086185>
- Boyet, A., De Simone, S., Ge, S., & Vilarrasa, V. (2023). Poroelastic stress relaxation, slip stress transfer and friction weakening controlled post-injection seismicity at the Basel Enhanced Geothermal System. *Communications Earth and Environment*, *4*, 104. <https://doi.org/10.1038/s43247-023-00764-y>
- Boyet, A., De Simone, S., & Vilarrasa, V. (2024). To bleed-off or not to bleed-off? *Geophysical Research Letters*, *51*(23), e2023GL107926. <https://doi.org/10.1029/2023GL107926>
- Byerlee, J. (1978). Friction of rocks. *Pure and Applied Geophysics*, *116*(4–5), 615–626. <https://doi.org/10.1007/BF00876528>
- Cappa, F., Scuderi, M. M., Collettini, C., Guglielmi, Y., & Avouac, J. P. (2019). Stabilization of fault slip by fluid injection in the laboratory and in situ. *Science Advances*, *5*(3), eaau4065. <https://doi.org/10.1126/sciadv.aau4065>
- De Barros, L., Cappa, F., Guglielmi, Y., Duboeuf, L., & Grasso, J. R. (2019). Energy of injection-induced seismicity predicted from in-situ experiments. *Scientific Reports*, *9*(1), 4999. <https://doi.org/10.1038/s41598-019-41306-x>
- Dieterich, J. H. (1979). Modeling of rock friction: 1. Experimental results and constitutive equations. *Journal of Geophysical Research*, *84*(B5), 2161–2168. <https://doi.org/10.1029/JB084iB05p02161>
- Ellsworth, W. L. (2013). Injection-induced earthquakes. *Science*, *341*(6142), 1225942. <https://doi.org/10.1126/science.1225942>
- Ellsworth, D., Spiers, C. J., & Niemeijer, A. R. (2016). Understanding induced seismicity. *Science*, *354*(6318), 1380–1381. <https://doi.org/10.1126/science.aal2584>
- Evans, K. F., Zappone, A., Kraft, T., Deichmann, N., & Moia, F. (2012). A survey of the induced seismic responses to fluid injection in geothermal and CO<sub>2</sub> reservoirs in Europe. *Geothermics*, *41*, 30–54. <https://doi.org/10.1016/j.geothermics.2011.08.002>

## Acknowledgments

This study is financially supported by the National Natural Science Foundation of China (12572462, 51774267, 42302316, and U22A20234).

- Galis, M., Ampuero, J. P., Mai, P. M., & Cappa, F. (2017). Induced seismicity provides insight into why earthquake ruptures stop. *Science Advances*, 3(12), eaap7528. <https://doi.org/10.1126/sciadv.aap7528>
- Garagash, D. I., & Germanovich, L. N. (2012). Nucleation and arrest of dynamic slip on a pressurized fault. *Journal of Geophysical Research*, 117(B10), B10310. <https://doi.org/10.1029/2012JB009209>
- Geng, Z. (2025). Supplementary data for the study of Cycled fluid injection limits maximum earthquake size by controlling the cadence of seismic moment release (Version 1) [Dataset]. *Mendeley Data*. <https://doi.org/10.17632/KVWNBPNRPWG>
- Goebel, T. H. W., & Brodsky, E. E. (2018). The spatial footprint of injection wells in a global compilation of induced earthquake sequences. *Science*, 361(6405), 899–904. <https://doi.org/10.1126/science.aat5449>
- Goodfellow, S. D., Maxwell, S. C., & Young, R. P. (2015). Hydraulic fracture energy budget: Insights from the laboratory. *Geophysical Research Letters*, 42(9), 3179–3187. <https://doi.org/10.1002/2015GL063093>
- Guglielmi, Y., Cappa, F., Avouac, J. P., Henry, P., & Elsworth, D. (2015). Seismicity triggered by fluid injection–induced aseismic slip. *Science*, 348(6240), 1224–1226. <https://doi.org/10.1126/science.aab0476>
- Häring, M. O., Schanz, U., Ladner, F., & Dyer, B. C. (2008). Characterisation of the Basel 1 enhanced geothermal system. *Geothermics*, 37, 469–495. <https://doi.org/10.1016/j.geothermics.2008.06.002>
- Ji, J. Y., Wang, L., Hofmann, H., Kwiatek, G., & Dresen, G. (2022). High-rate fluid injection reduces the nucleation length of laboratory earthquakes on critically stressed faults in granite. *Geophysical Research Letters*, 49(23), e2022GL100418. <https://doi.org/10.1029/2022GL100418>
- Ji, Y., Hofmann, H., Duan, K., & Zang, A. (2022b). Laboratory experiments on fault behavior towards better understanding of injection-induced seismicity in geoenery systems. *Earth-Science Reviews*, 226, 103916. <https://doi.org/10.1016/j.earscirev.2022.103916>
- Ji, Y., Zhuang, L., Wu, W., Hofmann, H., Zang, A., & Zimmermann, G. (2021). Cyclic water injection potentially mitigates seismic risks by promoting slow and stable slip of a natural fracture in granite. *Rock Mechanics and Rock Engineering*, 54(10), 5389–5405. <https://doi.org/10.1007/s00603-021-02438-7>
- Kang, J. Q., Zhu, J. B., & Zhao, J. (2019). A review of mechanisms of induced earthquakes: From a view of rock mechanics. *Geomechanics and Geophysics for Geo-Energy and Geo-Resources*, 5, 171–196. <https://doi.org/10.1007/s40948-018-0094-3>
- Kim, K. H., Ree, J. H., Kim, Y. H., Kim, S., Kang, S. Y., & Seo, W. (2018). Assessing whether the 2017 Mw 5.4 Pohang earthquake in South Korea was an induced event. *Science*, 360(6392), 1007–1009. <https://doi.org/10.1126/science.aat6081>
- Kolawole, F., Johnston, C. S., Morgan, C. B., Chang, J. C., Marfurt, K. J., Lockner, D. A., et al. (2019). The susceptibility of Oklahoma’s basement to seismic reactivation. *Nature Geoscience*, 12(10), 839–844. <https://doi.org/10.1038/s41561-019-0440-5>
- Li, Z., Elsworth, D., & Wang, C. (2021). Constraining maximum event magnitude during injection-triggered seismicity. *Nature Communications*, 12(1), 1528. <https://doi.org/10.1038/s41467-020-20700-4>
- Mandal, R., & Lui, S. K. Y. (2022). Interdependent effects of fluid injection parameters on triggered aseismic slip and seismicity. *Scientific Reports*, 12(1), 20922. <https://doi.org/10.1038/s41598-022-25239-6>
- Maxwell, S. (2013). Unintentional seismicity induced by hydraulic fracturing. *CSEG Recorder*, 38, 40–49.
- McGarr, A. (1999). On relating apparent stress to the stress causing earthquake fault slip. *Journal of Geophysical Research*, 104(B2), 3003–3011. <https://doi.org/10.1029/1998JB900083>
- McGarr, A. (2014). Maximum magnitude earthquakes induced by fluid injection. *Journal of Geophysical Research: Solid Earth*, 119(2), 1008–1019. <https://doi.org/10.1002/2013JB010597>
- McGarr, A., & Barbour, A. J. (2018). Injection-induced moment release can also be aseismic. *Geophysical Research Letters*, 45(11), 5344–5351. <https://doi.org/10.1029/2018GL078422>
- McGarr, A., Bekins, B., Burkhardt, N., Dewey, J., Earle, P., Ellsworth, W., et al. (2015). Coping with earthquakes induced by fluid injection. *Science*, 347(6224), 830–831. <https://doi.org/10.1126/science.aaa0494>
- McLaskey, G. C., & Kilgore, B. D. (2013). Foreshocks during the nucleation of stick-slip instability. *Journal of Geophysical Research: Solid Earth*, 118(6), 2982–2997. <https://doi.org/10.1002/jgrb.50232>
- Niemz, P., Cesca, S., Heimann, S., Grigoli, F., von Specht, S., Hammer, C., et al. (2020). Full-waveform-based characterization of acoustic emission activity in a mine-scale experiment: A comparison of conventional and advanced hydraulic fracturing schemes. *Geophysical Journal International*, 222, 189–206. <https://doi.org/10.1093/gji/ggaa164>
- Raleigh, C. B., Healy, J. H., & Bredehoeft, J. D. (1976). An experiment in earthquake control at Rangely, Colorado. *Science*, 191(4233), 1230–1237. <https://doi.org/10.1126/science.191.4233.1230>
- Sáez, A., Passelègue, F., & Lecampion, B. (2025). Maximum size and magnitude of injection-induced slow slip events. *Science Advances*, 11, eadq0662. <https://doi.org/10.1126/sciadv.adq0662>
- van der Elst, N. J., Page, M. T., Weiser, D. A., Goebel, T. H. W., & Hosseini, S. M. (2016). Induced earthquake magnitudes are as large as (statistically) expected. *Journal of Geophysical Research: Solid Earth*, 121(6), 4575–4590. <https://doi.org/10.1002/2016JB012818>
- Violay, M., Di Toro, G., Nielsen, S., Spagnuolo, E., & Burg, J. P. (2015). Thermo-mechanical pressurization of experimental faults in cohesive rocks during seismic slip. *Earth and Planetary Science Letters*, 429, 1–10. <https://doi.org/10.1016/j.epsl.2015.07.054>
- Wang, L., Kwiatek, G., Renard, F., Guérin, S., Rybacki, E., Bohnhoff, M., et al. (2024). Fault roughness controls injection-induced seismicity. *Proceedings of the National Academy of Sciences of the United States of America*, 121(3), e2310039121. <https://doi.org/10.1073/pnas.2310039121>
- Wang, L., Kwiatek, G., Rybacki, E., Bohnhoff, M., & Dresen, G. (2020). Injection-induced seismic moment release and laboratory fault slip: Implications for fluid-induced seismicity. *Geophysical Research Letters*, 47(22), e2020GL089576. <https://doi.org/10.1029/2020GL089576>
- Wang, L., Kwiatek, G., Rybacki, E., Bonnelye, A., Bohnhoff, M., & Dresen, G. (2020). Laboratory study on fluid-induced fault slip behavior: The role of fluid pressurization rate. *Geophysical Research Letters*, 47(6), e2019GL086627. <https://doi.org/10.1029/2019GL086627>
- Yeo, I. W., Brown, M. R. M., Ge, S., & Lee, K. K. (2020). Causal mechanism of injection-induced earthquakes through the Mw 5.5 Pohang earthquake case study. *Nature Communications*, 11(1), 2614. <https://doi.org/10.1038/s41467-020-16408-0>
- Yu, J., Eijsink, A., Marone, C., Rivière, J., Shokouhi, P., & Elsworth, D. (2024). Role of critical stress in quantifying the magnitude of fluid-injection triggered earthquakes. *Nature Communications*, 15(1), 7893. <https://doi.org/10.1038/s41467-024-52089-9>
- Yu, P., Mali, A., Velaga, T., Bi, A., Yu, J., Marone, C., et al. (2024). Crustal permeability generated through microearthquakes is constrained by seismic moment. *Nature Communications*, 15(1), 2057. <https://doi.org/10.1038/s41467-024-46238-3>
- Zang, A., Yoon, J. S., Stephansson, O., & Heidbach, O. (2013). Fatigue hydraulic fracturing by cyclic reservoir treatment enhances permeability and reduces induced seismicity. *Geophysical Journal International*, 195(2), 1282–1287. <https://doi.org/10.1093/gji/ggt301>
- Zang, A., Zimmermann, G., Hofmann, H., Stephansson, O., Min, K. B., Kim, K. Y., et al. (2019). How to reduce fluid-injection-induced seismicity. *Rock Mechanics and Rock Engineering*, 52(2), 475–493. <https://doi.org/10.1007/s00603-018-1467-4>

- Zhu, J. B., Kang, J. Q., Elsworth, D., Xie, H. P., Ju, Y., & Zhao, J. (2021). Controlling induced earthquake magnitude by cycled fluid injection. *Geophysical Research Letters*, *48*(19), e2021GL092885. <https://doi.org/10.1029/2021GL092885>
- Zhuang, L., Kim, K. Y., Jung, S. G., Diaz, M., Min, K.-B., Zang, A., et al. (2019). Cyclic hydraulic fracturing of Pocheon granite cores and its impact on breakdown pressure, acoustic emission amplitudes and injectivity. *International Journal of Rock Mechanics and Mining Sciences*, *122*, 104065. <https://doi.org/10.1016/j.ijrmmms.2019.104065>

### References From the Supporting Information

- Aki, K. (1966). Generation and propagation of G waves from the Niigata earthquake of June 16, 1964. Part 1. A statistical analysis. *Bulletin of the Earthquake Research Institute*, *44*, 23–72.
- Hanks, T. C., & Kanamori, H. (1979). A moment magnitude scale. *Journal of Geophysical Research*, *84*(B5), 2348–2350. <https://doi.org/10.1029/JB084iB05p02348>
- Kanamori, H., & Anderson, D. L. (1975). Theoretical basis of some empirical relations in seismology. *Bulletin of the Seismological Society of America*, *65*, 1073–1095.
- Kanamori, H. (1978). Quantification of earthquakes. *Nature*, *271*(5644), 411–414. <https://doi.org/10.1038/271411a0>
- Linker, M. F., & Dieterich, J. H. (1992). Effects of variable normal stress on rock friction: Observations and constitutive equations. *Journal of Geophysical Research*, *97*(B4), 4923–4940. <https://doi.org/10.1029/92jb00017>
- Liu, B., Geng, Z., Kang, Y., Liu, X., Zhou, Y., Liu, Q., et al. (2024). Fault slip behaviors and frictional stability controlled by particle size of fault gouge under fluid injection. *International Journal of Rock Mechanics and Mining Sciences*, *183*, 105919. <https://doi.org/10.1016/j.ijrmmms.2024.105919>